Nuclear Inst. and Methods in Physics Research B 445 (2019) 63–68

Contents lists available at ScienceDirect

Nuclear Inst. and Methods in Physics Research B

journal homepage: www.elsevier.com/locate/nimb

Co-60 gamma irradiation influences on device characteristics of n-SnO_2/p-Si heterojunction diodes

Senol Kaya[a,*], Saleh Abubakar[a,b], Ercan Yilmaz[a,b]

[a] Center for Nuclear Radiation Detectors Research and Applications, BAIBU, 14280 Bolu, Turkey
[b] Physics Department, Bolu Abant Izzet Baysal University, 14280 Bolu, Turkey

ARTICLE INFO

Keywords:
Heterojunction
Microelectronics
Ionizing radiation
SnO_2 thin film
Radiation effect
Radiation degradation
XPS

ABSTRACT

Gamma irradiation induced modifications on the structural, morphological, and electrochemical characteristics of the n-SnO_2/p-Si heterojunction diodes incorporating their influences on the electrical properties of diode have been systematically studied. The results indicate that irradiation exposure improves the crystallographic structure of the SnO_2 layer as expected but, reduce the device capacitance due to changes in the dielectric characteristics of the SnO_2. In addition, the surface roughness of the SnO_2 thin films become smoother as the irradiation exposures enhanced. On the other hand, low dose irradiation exposure generates the local heating that neutralizes a portion of the dangling bonds which are especially close to the interface between SnO_2 and Si. Hence, interface state density decreases after low dose irradiation exposure. However, high irradiation doses create a large number of oxygen vacancies and interstitial defect. These generated defect sites lead to changes on the barrier potential and conduction mechanism of the diode. It can be concluded that complex irradiation induced mechanism has been observed for SnO_2/Si heterojunction diodes. Any irradiation-induced changes on the film structures and electrochemical parameters directly affect the electrical responses of the diodes.

1. Introduction

Owing to the continuous development of microelectronic technology, researchers have devoted great efforts to explore new promising materials in order to improve the device performance for future technology. Thus, various insulating and wide band-gap semiconducting oxide materials such as Bismuth Ferrite Oxides ($BiFeO_3$) [1], Yttrium Oxide (Y_2O_3) [2,3], Hafnium Oxide (HfO_2) [4], Titanium Oxide (TiO_2) [5], Zinc Oxide (ZnO) [6] etc., have been investigated by researchers to improve device performance for various applications. Among these materials, wide band-gap semiconductor Tin Oxide (SnO_2) [7] with n-type electrical conductivity in the presence of oxygen vacancy is one of the unique materials for the wide range applications including the gas sensor, photovoltaic, and optoelectronics [8–14]. There exist many studies on structural, optical and electrical properties of promising oxide materials but only a few of the device responses with these materials have been investigated under irradiation environment [15–19]. The present studies have depicted that initial device characteristics may be significantly changed by irradiation exposures due to irradiation-induced effects on the core oxide material, e.g., generation of the defect sites, trapped charges, variations on the crystalline structure etc. [4,15,20,21]. Hence, the possible variations on the device characteristics under irradiation exposures should be systematically investigated for development of reliable oxide-based devices. In this study, gamma ray-irradiation influence on the structural, morphological, chemical properties of n-SnO_2/p-Si heterojunctions and their correlations with the electrical features of SnO_2 based devices have been systematically investigated. The irradiation-induced effects on the crystallography and morphology of the SnO_2 films have been designated by analyzing the X-ray diffraction (XRD) and Atomic Force Microscopy (AFM) measurements before and after irradiation respectively, while the electrochemical behaviors have been analyzed by X-ray Photoelectron Spectroscopy (XPS). Furthermore, Capacitance-Voltage (C-V), Conductance – Voltage (G/ω-V) and Current Density-voltage (J-V) measurements have been performed for analyzing the irradiation-induced effects on electrical characteristics of the fabricated Al/n-SnO_2/p-Si devices.

2. Experimental details

A 500 μm thick p-type Silicon (Si) wafer with a resistivity of 1–5 Ohm-Cm was used as a substrate for deposition of the Tin Oxide (SnO_2) layer. Before the deposition of the SnO_2 layer, Si wafer was cleaned by following the standard RCA cleaning process. Electron Beam

* Corresponding author.
E-mail address: senolkaya52@gmail.com (S. Kaya).

https://doi.org/10.1016/j.nimb.2019.03.013
Received 1 October 2018; Received in revised form 6 February 2019; Accepted 8 March 2019
Available online 13 March 2019
0168-583X/

Evaporation (E-Beam) technique was used for the deposition of the SnO_2. The pressure of the E-Beam chamber was adjusted to be 5×10^{-4} Pascal. The e-beam was focused on SnO_2 granular target to grown oxide layer onto Si. The deposition rate was approximately 1.0 nm s^{-1}. The thickness of the Tin Oxide layer was measured to be 110 nm by using Spectroscopic Reflectometer. The fabricated SnO_2/Si samples were annealed at 400 °C for one hour under nitrogen gas ambient at atmospheric pressure. Afterward, the annealed samples (n-SnO_2/p-Si) were separated into six pieces. Three of these samples were transformed to heterojunction diodes. The heterojunction diodes were fabricated by depositing Aluminum (Al) metal onto the front side of the annealed n-SnO_2/p-Si samples using a shadow mask with circular dots of 1.5 mm diameter. The fabricated Al/n-SnO_2/p-Si samples were divided into three groups. In each group, there is one heterojunction thin film (n-SnO_2/p-Si) and one heterojunction diode (Al/n-SnO_2/p-Si). The first group was separated as-deposited (virgin), while the second and third group samples were irradiated under Co-60 gamma irradiator at a dose rate of approximately 417 Gy per hour at the TAEK, Ankara. The second group samples were exposed to the totally 1000 Gy called as low dose exposed samples, and the third group samples were exposed to the totally 4000 Gy called high dose exposed samples in this study. The irradiation effects on crystallographic and morphological characteristics of the films have been analyzed by XRD and AFM, respectively. Radiation-induced chemical variations on the film structure have been discussed by XPS analysis. In order to explore the irradiation-induced changes on electrical properties of the devices, high frequency (1 MHz) C-V, G/ω-V and J-V characteristics of the heterojunction diodes have been measured and analyzed.

3. Results and discussion

3.1. Irradiation induced changes on the structural and morphological characteristics of the Tin Oxide

The XRD patterns of the SnO_2 thin films prior to and after gamma irradiation exposures are shown in Fig. 1. With vaguely seen and low intensive peaks, a poorly crystallized SnO_2 thin film structure has been obtained for the pristine sample. After low dose irradiation exposure, a sharp increment in the intensities of the peaks has been observed. The obtained peaks were analyzed using the International Centre for Diffraction Data (ICDD) base and patterns are matched with the orthorhombic phase of the SnO_2 (ICDD No: 29-1484 and 78-1063). Further increase in the radiation exposure also slightly improves the peak intensities and does not form the new sub-peaks in comparison with XRD patterns measured after low dose exposure. This means that radiation exposure continuously enhances the crystalline structure of the SnO_2 without forming secondary phases. On the other hand, peak angles slightly shift to higher angles. The peak angles of the most intense peak of (2 0 4) plane before and after gamma irradiation exposures are listed in Table 1. These shifts in the peak angle are due to the displacement of atoms on the film structure under irradiation exposure [22]. Moreover, the peak angle of the (2 0 4) plane locates at 44.52° for the standard bulk SnO_2 layer obtained from ICDD database. The continuous shifts toward higher angle demonstrate that the possible stress on the film structure increases with irradiation exposures. Irradiation-induced modifications on the SnO_2 crystalline having tetragonal phase have been also observed in the literature [23,24]. It is known that different phases of the same material may exhibit different characteristics under similar conditions [25,26]. However, it is seen that the crystallographic behavior of SnO_2 is strongly dependent on the gamma irradiation exposures for both orthorhombic and tetragonal phases.

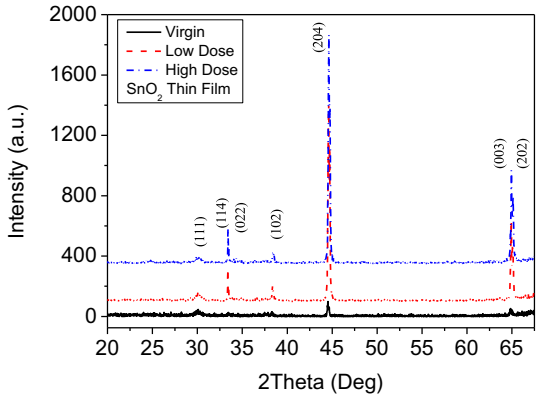

Fig. 1. The XRD spectra of SnO_2 thin films under gamma irradiation exposures.

In addition, the average grain size (P) of the films is also calculated using the well-known Scherrers' formula [27]. The broadening of the (2 0 4) peaks was used, during the grain size calculation. Hence, the full width half maximum (FWHM) and the calculated P values are tabulated in Table 1. It is observed that the FWHM narrowed, thus the average grain sizes of the sample enhance after irradiation exposures, particularly after low dose exposure. The evolutions on the crystalline structure and grain size of the films can be attributed to irradiation-generated local-heating of the Nano-scale particles, which may also affect the local stress-strain between the grains [4,23,28]. The presence of local heating may cause coalition of a smaller grain in a larger cluster. Thus, reorganization of the grains may cause variations in lattice volume and/or parameters.

The morphological changes after irradiation exposures have been analyzed by AFM images of the samples shown in Fig. 2(a)–(c). A slight change has been observed after irradiation exposures on the surface morphology on the SnO_2 thin films. Although the variations on the film morphology, no hillock and crank formation was observed. This observation points out that the surface strain/stress generated by irradiation exposure were not too high to damage the surface morphology [22]. On the other hand, the surface roughness of the images was analyzed using the AFM software and the Root Mean Square (RMS) roughness values for the SnO_2 films prior to after irradiation exposures are listed in Table 1. The surface roughness of thin films became smoother as the irradiation exposures increased [29]. Together with ionization and atomic displacement effects, ionizing irradiation also causes lattice vibration in the structure. During the irradiation transfer its energy to lattice points, significant lattice vibration can be generated. These generated lattice vibration cause lattice phonon scattering, which releases local heating [22,30]. With the released local heating energy, the surface atoms may get enough energy to immigrate to the substrate regions [31]. This atomic motion may be the reason for the improvement of the surface morphology of the SnO_2 thin film.

3.2. Irradiation influence on electro chemical characteristics of SnO_2/Si thin film

The effects of irradiation on the chemical characteristics of n-SnO_2/p-Si heterojunction have been studied by analyzing the XPS spectra. The XPS spectra of the core levels of Tin (Sn) and Oxygen (O) depending on the irradiation exposures are shown in Fig. 3(a) and (b), respectively. All peaks are calibrated to C1s peak at 284.5 eV to remove the feasible impurity effect, during the XPS analysis. The calibrated XPS peaks were analyzed by de-convolution software and possible sub-oxidation states have been specified. The obtained sub-states are numbered and also depicted in Fig. 3(a) and (b). The essential parameters for these sub-states are listed in Table 1. Themlin et al. [32] assigned the positions of each binding energy (BE) of $Sn3d_{5/2}$ to 486.3 eV, 485.6 eV, and 483.8 eV for Sn^{4+}, Sn^{2+}, and Sn^0, respectively. In addition, Choi at. al. [33] assigned that the positions of each binding energy of the O1s to 530.5 eV, and 530.15 eV for O^- and O^{2-} pieces, respectively. These findings are actually the oxidation states of the O^- (O–Sn^{4+}) in the oxygen-deficient SnO_{2-x}, and O^{2-} (O–Sn^{2+}) in SnO_2 [33]. Sn^0 denotes the metallic bonding states of Sn-Sn or Sn-Si

Table 1
Some structural and electrochemical characteristics of n-SnO_2/p-Si heterostructure before and after gamma irradiation exposures.

Sample	Peak Ang. (degree)	FWHM (degree)	Grain size (nm)	RMS roughness (nm)	[O]/[Sn] ratio	Sn states (eV)		O states (eV)	
						Peak No:1	Peak No:2	Peak No:1	Peak No:2
Virgin	44.55	0.345	24.86	12.80	1.10	485.98	485.50	529.81	529.62
Low Dose	44.59	0.259	33.11	11.51	1.12	486.02	486.13	529.87	530.13
High Dose	44.62	0.241	35.62	10.92	1.09	485.84	486.35	529.90	529.97

containing bonds. In the present study, the first sub-peaks of $Sn3d_{5/2}$ peak locates at 485.98 eV and O1s peak locates at 529.81 eV, while the second sub peaks of $Sn3d_{5/2}$ peak locates at 485.50 eV and O1s peak locates at 529.62 eV for the virgin samples. The BEs of the Sn and O peaks locate the lower values than stoichiometric SnO_2 compounds. The first sub-peaks of virgin samples can be attributed to the oxygen-deficient SnO_2 (SnO_{2-x}) bonds, while the second sub-peaks of virgin samples can be attributed to the metallic Sn-Sn and/or Sn-Si bonds. In addition, the intensity ratio has also depicted that the SnO_{2-x} is the dominant phase in the structure. Hence, this initial investigation has demonstrated that the oxygen-deficient (poor) SnO_2 layer has been fabricated in this present work. When SnO_2/Si films exposed to the low dose irradiation, the BE of Sn and O shift toward higher values and the intensity of the SnO_{2-x} peak enhances. It is also seen that the sub-states of the Sn-Si and/or Sn-Sn have not been observed. The BE shift to higher values can be attributed to either oxidation of the metallic bonds thanks to the incorporation of oxygen where oxygen vacancies present [4], or displacement of atoms in the disordered regions especially valid for the rise in the interstitial defects in the structure [34,35]. On the other hand, when the sample exposed to the high radiation doses, the BE of the Sn and O states in the SnO_{2-x} slightly shift toward lower energies and intensities of the related peaks decrease. However, the second sub-peaks shift toward higher BE, especially Sn^{2+} exceeds the 486.30 eV where stoichiometric SnO_2 bonds present. Together with intensity rise, large BE shift of Sn^{2+} points out the interstitial defects formation is dominant in the high irradiation dose exposure [34]. The lower BE shift indicates that bonds between Sn and O are broken. Thus, more metallic bonds are formed [4,22], e.g., O═Sn═O bonds can be transformed into more metallic Sn═O bonds. The broken bonds in the structure may enhance the oxygen-deficient SnO_{2-x} bonds which may affect the electrical characteristics of the devices. With high continuous irradiation energy, these oxygen-deficient bonds and other minor SnO_2 phases move towards disordered regions which enhance the interstitial defects. The theoretical report shows that the enhancement of the

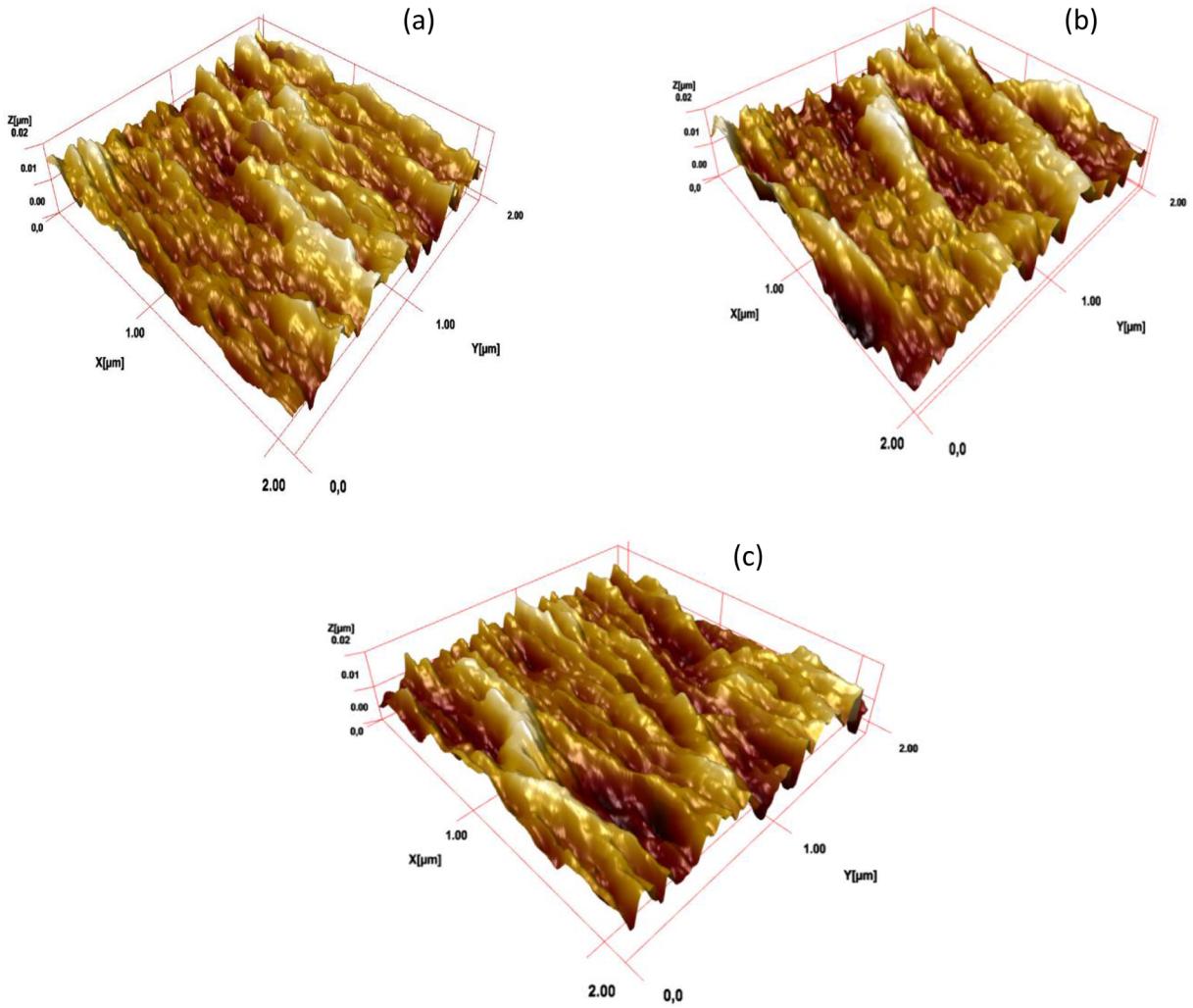

Fig. 2. AFM measurements of the SnO_2 thin films for (a) pristine, (a) low and (c) high dose exposed samples.

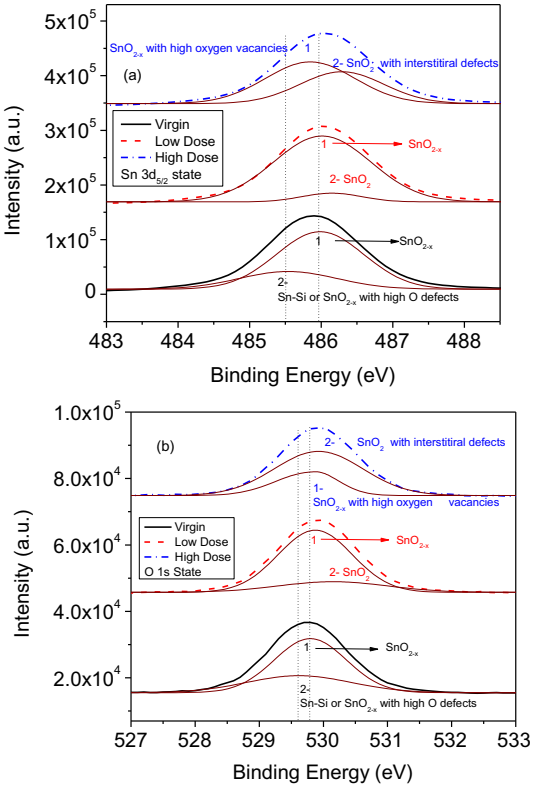

Fig. 3. Photoelectron spectra of a-) Sn3d and b-) O1s core levels of the pristine and irradiated samples.

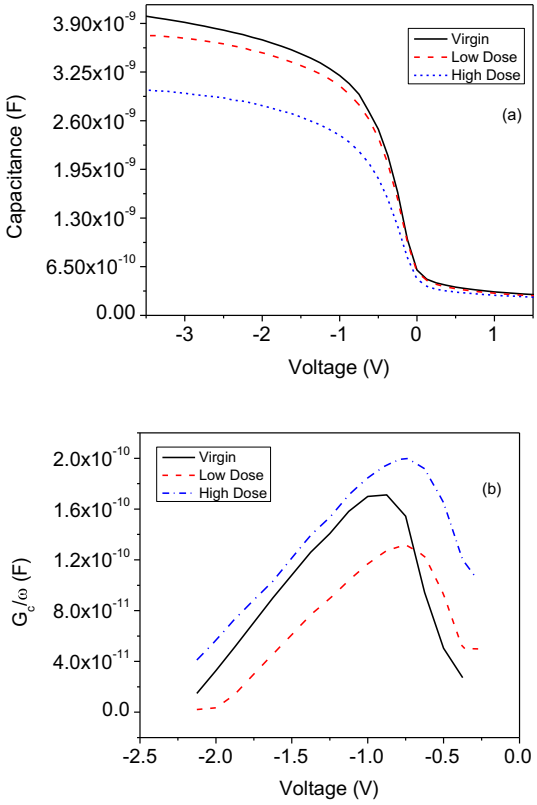

Fig. 4. Radiation-induced -) C-V and b-) G/ω-V curves of Al/n-SnO_2/p-Si heterojuction diodes.

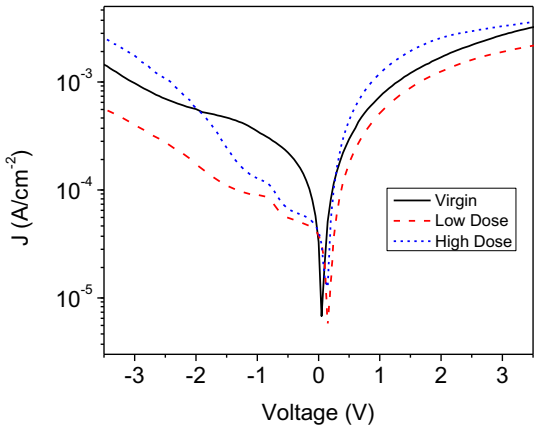

Fig. 5. Current density characteristics of Al/n-SnO_2/p-Si heterojuction diodes before and after gamma irradiation exposures.

oxygen-related interstitial defects decrease the current conduction characteristics of the SnO_2 layer, while the oxygen-related vacancy enhances the conduction characteristics of the device [35]. Hence, the atomic ratios of O over Sn were estimated prior to after the irradiation exposure via the XPS software. The estimated net O/Sn ratios are listed in Table 1. It has been seen that O concentrations on the film structure enhance after low dose irradiation exposure, which may be pointing out that the oxidation of the metallic bond occurs more efficiently rather than formation of the interstitial defects because net oxygen concentration should be almost constant for the formation of the oxygen-related interstitial defects. Thus, the binding energy shift towards higher values after low dose exposure can be attributed to the diffusion of the Oxygen present at the room atmosphere which is pulled into the sample by radiation generated local heating. On the other hand, the decreasing of the O concentration after high dose irradiation exposure is demonstrating both oxygen vacancies and interstitial defects in the structure enhanced. These defects may cause enhancement in the current conduction characteristics of the diode [35,36].

3.3. Irradiation influence on the electrical characteristics of Al/n-SnO_2/p-Si heterojunction devices

The electrical device performances under gamma irradiation exposures have been studied by analyzing the capacitance, conductance, and current density characteristics of the devices. In this view, the C-V and G/ω-V curves are depicted in Fig. 4(a) and (b), respectively, while J-V measurements are depicted in Fig. 5 prior to after irradiation exposures. The series resistance corrections (not shown here) have been performed for the capacitance and conductance characteristics shown in Fig. 4(a) and (b) in order to get real device characteristics [37]. The capacitance distribution of the semiconducting SnO_2 layer is particularly important for the conduction speed of future devices. The capacitance characteristics of the device in Fig. 4(a) significantly decrease with increasing the irradiation exposures. Selçuk et al. have reported a similar reduction on the capacitance curves and the reasons for this reduction were basically attributed to leakage through the oxide layers [38]. However, in the present study, no significant dependence between the capacitance curves (seen in Fig. 4(a)) and leakage current density characteristics (see $-0.3\ V < J < 0.3\ V$ in Fig. 5) have been observed. In other words, capacitance curves are continuously decreased with an increase in the irradiation exposures, while leakage current density exhibits variation depending on the irradiation exposures. Clausius–Mossotti relation [39,40] explain the relation between the dielectric constant (k), molar volume (V_m) and molecular polarizability (a) of a material [$k = (V_m + 2a/3)/(V_m - a/3)$]. It describes that any changes in the molecular volume owing to variations on the crystalline structure of the material may affect the dielectric constant [40,41]. The molecular polarizability contribution to dielectric constant is almost the same. Because, no any phase change was observed in XRD analysis.

Table 2
Some electrical characteristics of the n-SnO_2/p-Si heterostructure before and after gamma irradiation exposures.

Sample	G/ω_{max} ($\times10^{-10}$F)	C ($\times10^{-9}$F)	D_{it} ($\times10^{11}$ cm^{-2})	I_o ($\times10^{-7}$ A)	Ideality factor (n)	ϕ_b (eV)
Virgin	1.75	3.09	1.83	3.85	1.94	0.65
Low D.	1.13	2.91	1.79	9.17	3.12	0.62
High D.	2.01	2.19	14.6	7.90	4.00	0.63

However, during the XRD analysis, we have observed that the peak angle shift toward higher angles. These peak shifts demonstrate that lattice volume changed with irradiation exposures. Hence, the variation in the capacitance may be attributed to molar volume (V_m) fluctuation of the SnO_2 layer which may affect the dielectric constant. In addition, the irradiation influences on the interface state density of devices have been studied by using the peak values in the conductance characteristics in Fig. 4(b). The D_{it} of the SnO_2/Si interface before and after gamma irradiation exposures were calculated using well-known Hill and Coleman technique [42]. The essential parameters used in the D_{it} calculation and calculated D_{it} values are listed in Table 2. The D_{it} values of devices decrease after low dose irradiation exposure, while it enhances after the high dose irradiation exposure. The decrement of D_{it} value after low dose irradiation exposures are indicating the treatment effect of irradiation. As mentioned in the XPS analysis, local heating may be generated by irradiation which may cause the oxidation of the dangling bonds in the structure. A small capacitance shift to lower voltage site is maybe also associated with the generation of positive defects during neutralization of oxygen vacancies. However, the rise in the D_{it} value after high dose irradiation exposures depicted that the bond breaking mechanism of the irradiation become more dominant rather than a treatment effect.

Thermionic emission (TE) is a most dominant carrier conduction mechanism in the heterojunction devices. Also, it is an ideal approach to describe the experimental current through the barrier potential in the diode [43,44]. In this theory, the forward current, which is obtained when the positive voltage is applied to p-Si, can be denoted [45,46]

$$I = I_0\left[\exp\left(\frac{qV}{nkT}\right) - 1\right] \quad (1\text{-a})$$

$$I_0 = AA^*T^2\exp\left(-\frac{q\varphi_b}{kT}\right) \quad (1\text{-b})$$

$$\frac{1}{n} = \frac{kT}{q}\left(\frac{d\ln I}{dV}\right) \quad (1\text{-c})$$

$$\varphi_b = \frac{kT}{q}\ln\left(\frac{AA^*T^2}{I_o}\right) \quad (1\text{-d})$$

where I_0 is the reverse saturation current, V is the applied voltage, I is the current, k is the Boltzmann constant, T is the ambient temperature, A is the front contact area, A^* (32 A $cm^{-2}K^{-2}$ for p-type Si) is the Richardson constant and ϕ_b is the barrier potential, n is a dimensionless ideality factor. The I_0 is determined from the intercept semilogarithmic current-voltage (ln(I)-V, not shown here) curve on the current axis and the values of the I_o are listed in Table 2. The rise on the I_o value result of the generation of the new defect site where mobile charges may contribute the leak current flow.

On the other hand, the n should be one where the TE is the dominant transport mechanism for an ideal diode behavior. The n values have calculated from the slope of the linear region of the forward bias of ln(I)-V curves. The calculated n values are given in Table 2. In real device applications, the n value is in the range between 1 and 2. When n values exceed the 2, it demonstrates that TE over the barrier is not dominant [43] and this shows the contribution of the other conduction mechanisms to the carrier transport in the junction region become more effective such as tunneling and recombination [47]. In addition, when n values approach to 4 or higher value than 4, it means that the current transport mechanism is dominated by defect-assisted tunneling and space charge current at the device [48]. As seen from Table 2, the n value was 1.94 which is indicating that TE is a dominant transport mechanism. However, with irradiation exposures, the n values continuously increase and exceed to 4 after a high dose of gamma radiation exposure. These variations on the n values depict that irradiation exposures significantly influence the current transport mechanism of the device. The irradiation exposures may also degrade the ϕ_b of the device. Using the I_o, the ϕ_b of devices was also calculated [49] and their values are given in Table 2. The ϕ_b values significantly decrease after low dose radiation exposures and very slight increment was observed following the high radiation exposures. These changes can be also attributed to the inhomogeneous interfacial layer formation and the irradiation generated surface state [47,48,50]. In other words, increases in the oxygen vacancies in the oxide bonds and presence of the interstitial defect formation.

On the other hand, the J-V characteristics exhibit variation under forward and reverse bias regimes. When absolute values of the applied bias are higher than 0.4 V, the J value almost linearly changes with bias owing to the presence of the series and shunt resistance [51]. Particularly when applied bias is lower than −0.4 V, the J characteristics deviate from linear behavior. These fluctuations become more obvious for irradiated samples. These observed deviations may be due to the inhomogeneous distribution of the series resistance (R_s) effect, interface states (D_{it}) and the presence of the parasitic layer at the SnO_2/Si interface [43,49]. In addition, the distributions of leakage regimes (J_g is from −0.3 V to +0.3 V) have been carefully discussed. The J_g under reverse voltage is a bit higher than the J value under a forward voltage at the similar absolute voltage especially for virgin and low dose exposed samples. These may be due to the different carrier under the different injection mode and conduction mechanism in the Al/SnO_2 and SnO_2/Si interface [52,53]. These differences may also be explained by the series resistance effects. It is known that series resistance is applied voltage dependent and its distribution may changes with irradiation exposures due to reordering and restructuring of radiation-induced defects densities, like, generation of the deficient bonds and/or interstitial defect formation [1,54]. Hence, the J_g values in reverse bias regimes are higher than the values in the forward bias regimes, this may be due to the applied voltage dependency of the R_s values which may significantly influence the device characteristics [15].

4. Conclusion

We have demonstrated that irradiation may improve the crystallographic structure and the surface roughness of the films. The changes in the crystalline structure may directly affect the dielectric specification of the SnO_2. The capacitance of the devices decreases with increase in irradiation doses due to the possible enhancement of the lattice volume. The electrochemical analysis, the distribution of the D_{it} value and the J-V characteristics have demonstrated that low irradiation doses may generate the local heating which may neutralize the some of dangling bonds. However, when irradiation doses are enhanced, the generation of the oxygen vacancies and interstitial defect densities significantly increase. Due to these generated defects, the barrier potential decrease and ideality factor of Al/n-SnO_2/p-Si heterojunction diodes significantly increase. In addition, defect-assisted tunneling becomes dominant conduction mechanisms than thermionic emission especially after high irradiation exposures, due to the enormous

generation of the defect sites. It can be concluded that irradiation may significantly change the structural and electrochemical characteristics of the SnO_2 layer which directly affect the electrical performance of the heterojunction diodes.

Acknowledgments

This work is supported by the Presidency of Turkey, Presidency of Strategy and Budget under Contract Number: 2016K121110, and in part by BAIBU under Contract number BAP. 2017.03.02.1153 Bolu, Turkey.

References

[1] S. Kaya, R. Lok, A. Aktag, J. Seidel, E. Yilmaz, Frequency dependent electrical characteristics of $BiFeO_3$ MOS capacitors, J. Alloy Compd. 583 (2014) 476–480.
[2] S. Abubakar, S. Kaya, H. Karacali, E. Yilmaz, The gamma irradiation responses of yttrium oxide capacitors and first assessment usage in radiation sensors, Sensor Actuat a-Phys. 258 (2017) 44–48.
[3] S. Abubakar, S. Kaya, A. Aktag, E. Yilmaz, Yttrium oxide nanostructured thin films deposited by radio frequency sputtering: the annealing optimizations and correlations between structural, morphological, optical and electrical properties, J. Mater. Sci.-Mater Electron. 28 (2017) 13920–13927.
[4] S. Kaya, I. Yıldız, R. Lok, E. Yılmaz, Co-60 gamma irradiation influences on physical, chemical and electrical characteristics of HfO_2/Si thin films, Radiat. Phys. Chem. 150 (2018) 64–70.
[5] S. Abubakar, E. Yilmaz, Optical and electrical properties of E-Beam deposited TiO_2/Si thin films, J. Mater. Sci.-Mater. Electron. 29 (2018) 9879–9885.
[6] M. Guziewicz, R. Schifano, E. Przezdziecka, J.Z. Domagala, W. Jung, T.A. Krajewski, E. Guziewicz, n-ZnO/p-4H-SiC diode: structural, electrical, and photoresponse characteristics, Appl. Phys. Lett. 107 (2015) 101105.
[7] A.M. Ganose, D.O. Scanlon, Band gap and work function tailoring of SnO_2 for improved transparent conducting ability in photovoltaics, J. Mater. Chem. C 4 (2016) 1467–1475.
[8] M. Kwoka, L. Ottaviano, M. Passacantando, S. Santucci, J. Szuber, XPS depth profiling studies of L-CVD SnO_2 thin films, Appl. Surf. Sci. 252 (2006) 7730–7733.
[9] S. Ferrere, A. Zaban, B.A. Gregg, Dye sensitization of nanocrystalline tin oxide by perylene derivatives, J. Phys. Chem. B 101 (1997) 4490–4493.
[10] J. Kaur, R. Kumar, M.C. Bhatnagar, Effect of indium-doped SnO_2 nanoparticles on NO2 gas sensing properties, Sensor Actuat. B-Chem. 126 (2007) 478–484.
[11] W. Lee, K. Hong, Y. Park, N.H. Kim, Y. Choi, J. Park, Surface and sensing properties of PE-ALD SnO_2 thin film, Electron. Lett. 41 (2005) 475–477.
[12] D.M. Priyadarshini, R. Mannam, M.S.R. Rao, N. DasGupta, Effect of annealing ambient on SnO_2 thin film transistors, Appl. Surf. Sci. 418 (2017) 414–417.
[13] R.E. Presley, C.L. Munsee, C.H. Park, D. Hong, J.F. Wager, D.A. Keszler, Tin oxide transparent thin-film transistors, J. Phys. D Appl. Phys. 37 (2004) 2810–2813.
[14] J.Y. Kim, B. Bae, E.J. Yun, Effects of post-annealing on the electrical properties of sputter-deposited SnO thin-film transistors, Sci. Adv. Mater. 8 (2016) 272–277.
[15] S. Kaya, E. Yilmaz, Influences of Co-60 gamma-ray irradiation on electrical characteristics of Al_2O_3 MOS capacitors, J. Radioanal. Nucl. Chem. 302 (2014) 425–431.
[16] S. Kaya, E. Yilmaz, A. Aktag, J. Seidel, Characterization of interface defects in $BiFeO_3$ metal-oxide-semiconductor capacitors deposited by radio frequency magnetron sputtering, J. Mater. Sci.-Mater. Electron. 26 (2015) 5987–5993.
[17] S. Kaya, E. Yilmaz, A. Kahraman, H. Karacali, Frequency dependent gamma-ray irradiation response of Sm_2O_3 MOS capacitors, Nucl. Instrum. Meth B 358 (2015) 188–193.
[18] R. Lok, S. Kaya, H. Karacali, E. Yilmaz, A detailed study on the frequency-dependent electrical characteristics of Al/$HfSiO_4$/p-Si MOS capacitors, J. Mater. Sci. Mater. Electron. 27 (2016) 13154–13160.
[19] R. Lok, S. Kaya, E. Yilmaz, Thermal phase separation of $ZrSiO_4$ thin films and frequency-dependent electrical characteristics of the Al/$ZrSiO_4$/p-Si/Al MOS capacitors, Semicond Sci. Tech. 33 (2018) 055007.
[20] S. Lotfy, A. Atta, E. Abdeltwab, Comparative study of gamma and ion beam irradiation of polymeric nanocomposite on electrical conductivity, J. Appl. Polym. Sci. 135 (2018).
[21] A.G. El-Shamy, W.M. Attia, K.M. Abd El Kader, Enhancement of the conductivity and dielectric properties of PVA/Ag nanocomposite films using gamma irradiation, Mater. Chem. Phys. 191 (2017) 225–229.
[22] S. Kaya, E. Yilmaz, Modifications of structural, chemical, and electrical characteristics of Er_2O_3/Si interface under Co-60 gamma irradiation, Nucl. Instrum. Method B 418 (2018) 74–79.
[23] N. Lavanya, C. Sekar, A.C. Anithaa, N. Sudhan, K. Asokan, A. Bonavita, S.G. Leonardi, G. Neri, Investigations on the effect of gamma-ray irradiation on the gas sensing properties of SnO_2 nanoparticles, Nanotechnology 27 (2016) 385502.
[24] K.M. Abhirami, R. Sathyamoorthy, K. Asokan, Structural, optical and electrical properties of gamma irradiated SnO thin films, Radiat. Phys. Chem. 91 (2013) 35–39.
[25] M.Q. Fu, Z.Q. Tang, X. Li, Z.Y. Ning, D. Pan, J.H. Zhao, X.L. Wei, Q. Chen, Crystal phase- and orientation-dependent electrical transport properties of InAs nanowires, Nano Lett. 16 (2016) 2478–2484.
[26] W. Zhang, H.B. Cheng, Q. Yang, F.R. Hu, J. Ouyang, Crystallographic orientation dependent dielectric properties of epitaxial $BaTiO_3$ thin films, Ceramics Int. 42 (2016) 4400–4405.
[27] F. Karaboga, H. Yetis, M. Oz, I. Belenli, Effect of different-sized h-BN nano-particles on some properties of MgB_2 superconductors, J. Mater. Sci. Mater. Electron. 27 (2016) 8512–8517.
[28] M. Ishfaq, M.R. Khan, A. Ali, S. Bhardwaj, C. Cepek, A.S. Bhatti, Optical and electrical characteristics of 17 keV X-rays exposed TiO2 films and Ag/TiO_2/p-Si MOS device, Mater. Sci. Semicon Process. 63 (2017) 107–114.
[29] N.A.N. Azmy, H. Abdullah, N.M. Naim, A.A. Hamid, S. Shaari, W.H.M.W. Mokhtar, Gamma irradiation effect on the structural, morphology and electrical properties of ZnO-CuO doped PVA nanocomposite thin films for Escherichia coli sensor, Radiat. Phys. Chem. 103 (2014) 108–113.
[30] P. Laha, I. Banerjee, P.K. Barhai, A.K. Das, V.N. Bhoraskar, S.K. Mahapatra, Effects of 6 MeV electron irradiation on the electrical properties and device parameters of Al/Al_2O_3/TiO2/n-Si MOS capacitors, Nucl. Instrum. Method B 283 (2012) 9–14.
[31] D. Kim, S. Kim, Effect of secondary ion beam energy and oxygen partial pressure on the structural, morphological and optical properties of ITO films prepared by DMIBD technique, Surf. Coat Technol. 154 (2002) 204–208.
[32] J.M. Themlin, M. Chtaib, L. Henrard, P. Lambin, J. Darville, J.M. Gilles, Characterization of tin oxides by X-Ray-photoemission spectroscopy, Phys. Rev. B 46 (1992) 2460–2466.
[33] G. Choi, L. Satyanarayana, J. Park, Effect of process parameters on surface morphology and characterization of PE-ALD SnO_2 thin films for gas sensing, Appl. Surf. Sci. 252 (2006) 7878–7883.
[34] I.G. Madiba, N. Emond, M. Chaker, F.T. Thema, S.I. Tadadjeu, U. Muller, P. Zolliker, A. Braun, L. Kotsedi, M. Maaza, Effects Of gamma irradiations on reactive pulsed laser deposited vanadium dioxide thin films, Appl. Surf. Sci. 411 (2017) 271–278.
[35] J.F. Yan, Z.Y. Zhang, F.C. Zhang, J.N. Yun, W. Zhao, Z.H. Deng, The first-principles calculation of the effects oxygen defect on the electronic structure of SnO2, 2008 2nd IEEE International Nanoelectronics Conference, Vols 1-3. (2008) 645.
[36] M. Ding, Y.H. Cheng, X. Liu, X.L. Li, Total dose response of hafnium oxide based metal-oxide-semiconductor structure under gamma-ray irradiation, IEEE Trans. Dielectr. Electron. Insult. 21 (2014) 1792–1800.
[37] S. Kaya, E. Yilmaz, A comprehensive study on the frequency-dependent electrical characteristics of Sm_2O_3 MOS capacitors, IEEE T Electron. Dev. 62 (2015) 980–987.
[38] A.B. Selcuk, S.B. Ocak, O.F. Yuksel, Effects of gamma irradiation on dielectric characteristics of SnO_2 thin films, Nucl. Instrum. Meth A 594 (2008) 395–399.
[39] E. Talebian, M. Talebian, A general review on the derivation of Clausius-Mossotti relation, Optik 124 (2013) 2324–2326.
[40] V. Singh, N. Shashank, D. Kumar, R.K. Nahar, Effects of heavy-ion irradiation on the electrical properties of rf-sputtered HfO_2 thin films for advanced CMOS devices, Radiat. Effect Defect Solids 167 (2012) 204–211.
[41] K. Tomida, K. Kita, A. Toriumi, Dielectric constant enhancement due to Si incorporation into HfO_2, Appl. Phys. Lett. 89 (2006) 142902.
[42] W.A. Hill, C.C. Coleman, A single-frequency approximation for interface-state density determination, Solid State Electron. 23 (1980) 987–993.
[43] M. Terlemezoglu, O. Bayrakli, H.H. Gullu, T. Colakoglu, D.E. Yildiz, M. Parlak, Analysis of current conduction mechanism in CZTSSe/n-Si structure, J. Mater. Sci. Mater Electron. 29 (2018) 5264–5274.
[44] S.M. Sze, K.N. Kwok, Physics of Semiconductor Devices, John Wiley & Sons, 2007.
[45] A.E. Rakhshani, Optoelectronic properties of p-n and p-i-n heterojunction devices prepared by electrodeposition of n-ZnO on p-Si, J. Appl. Phys. 108 (2010) 094502.
[46] O. Bayrakli, M. Terlemezoglu, H.H. Gullu, M. Parlak, Deposition of CZTSe thin films and illumination effects on the device properties of Ag/n-Si/p-CZTSe/In heterostructure, J. Alloys Compd. 709 (2017) 337–343.
[47] M. Kaleli, M. Parlak, C. Ercelebi, Studies on device properties of an n-AgIn5Se8/p-Si heterojunction diode, Semicond Sci. Technol. 26 (2011) 105013.
[48] K. Mageshwari, S. Han, J. Park, Fabrication and characterization of a CuO/ITO heterojunction with a graphene transparent electrode, Semicond Sci. Technol. 31 (2016) 055004.
[49] H.H. Gullu, O. Bayrakli, D.E. Yildiz, M. Parlak, Study on the electrical properties of ZnSe/Si heterojunction diode, J. Mater. Sci. Mater. Electron. 28 (2017) 17806–17815.
[50] N.H. Al-Hardan, M.A.A. Hamid, N.M. Ahmed, R. Shamsudin, N.K. Othman, Ag/ZnO/p-Si/Ag heterojunction and their optoelectronic characteristics under different UV wavelength illumination, Sensor Actuat. A-Phys. 242 (2016) 50–57.
[51] S. Kaya, Evolutions on surface chemistry, microstructure, morphology and electrical characteristics of SnO_2/p-Si heterojuction under various annealing parameters, J. Alloys Compd. 778 (2019) 889–899.
[52] S.S. Jiang, G. He, Z.B. Fang, P.H. Wang, Y.M. Liu, J.G. Lv, M. Liu, Analysis of the electrical properties and current transportation mechanism of a metal oxide semiconductor (MOS) capacitor based on HfGdO gate dielectrics, J. Alloys Compd. 757 (2018) 288–297.
[53] T. Yu, C.G. Jin, Y.J. Dong, D. Cao, L.J. Zhuge, X.M. Wu, Temperature dependence of electrical properties for MOS capacitor with HfO_2/SiO_2 gate dielectric stack, Mater. Sci. Semicon Procecess. 16 (2013) 1321–1327.
[54] S. Kaya, A. Aktag, E. Yilmaz, Effects of gamma-ray irradiation on interface states and series-resistance characteristics of $BiFeO_3$ MOS capacitors, Nucl. Instrum. Method B 319 (2014) 44–47.